



The Abdus Salam  
International Centre for Theoretical Physics



---

**EMAS 2008**

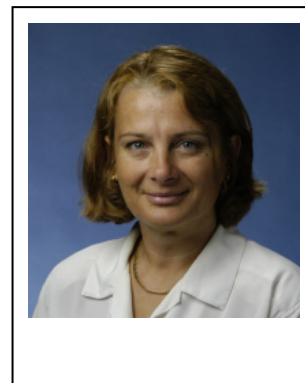
*8th EMAS Regional Workshop on*  
**Electron Probe Microanalysis  
of Materials Today**  
Practical Aspects  
including a session on  
synchrotron-based microanalysis

*19 - 22 April 2008*  
Adriatico Guesthouse  
The Abdus Salam International Centre for Theoretical Physics  
Trieste, Italy

**Book of Abstracts**

---

## SPATIALLY RESOLVED XRF, XAFS, AND XRD INVESTIGATIONS WITH MICROMETRE-SCALE RESOLUTION PERTAINING TO NUCLEAR WASTE DISPOSAL



**Melissa A. Denecke**<sup>1\*</sup>, B. Brendebach<sup>1</sup>, K. Dardenne<sup>1</sup>, F. Huber<sup>1</sup>, P. Michel<sup>1</sup>, T. Schäfer<sup>1</sup>, J. Rothe<sup>1</sup>, W. De Nolf<sup>2</sup>, K. Janssens<sup>2</sup>, K. Proost<sup>2</sup>, G. Falkenberg<sup>3</sup>, K. Rickers<sup>3</sup>, A. Somogyi<sup>4</sup>, R. Simon<sup>5</sup> and U. Noseck<sup>6</sup>

- 1 *Forschungszentrum Karlsruhe GmbH, Institut für Nukleare Entsorgung (INE)  
P.O. Box 3640, DE-76021 Karlsruhe, Germany*
  - 2 *University of Antwerp, Department of Chemistry, Micro- and Trace Analysis Centre (MiTAC)  
Campus Drie Eiken, Universiteitsplein 1, BE-2610 Antwerp-Wilrijk, Belgium*
  - 3 *Hamburger Synchrotronstrahlungslabor (HASYLAB) at DESY  
Notkestrasse 85, DE22603 Hamburg, Germany*
  - 4 *Synchrotron Soleil, Saint-Aubin  
P.O. Box 48, FR-91192 GIF-sur-Yvette, France*
  - 5 *Forschungszentrum Karlsruhe GmbH, Institut für Synchrotronstrahlung  
P.O. Box 3640, DE-76021 Karlsruhe, Germany*
  - 6 *Gesellschaft für Anlagen- und Reaktorsicherheit (GRS) mbH  
Theodor-Heuss Strasse 4, DE-38122 Braunschweig, Germany*
- \* *melissa@ine.fzk.de*

### ABSTRACT

Micro-focussed synchrotron radiation techniques to investigate determinant processes in actinide element transport in geological media are becoming an increasingly used tool in nuclear waste disposal research. There are a number of reasons for this but primarily they are driven by the need to characterize actinide speciation localized in components of heterogeneous natural systems. In this presentation, summaries of investigations using micro-focussed X-ray beams for characterisation of elemental distributions, of actinide oxidation states, and of mineral phases in samples originating from two different natural analogue sites and in post-tracer granite column studies are discussed. Such investigations are prerequisite to ensuring reliable assessment of the long term radiological safety for proposed nuclear waste disposal sites.

### INTRODUCTION

Over the past four years the “Institut für Nukleare Entsorgung” (INE, Institute for Nuclear Waste Disposal) at the “Forschungszentrum Karlsruhe” (FZK, Research Centre Karlsruhe) has embarked on a programme using micro-focussed synchrotron-generated X-rays for performing spatially resolved actinide speciation investigations. The goal of these investigations is to identify and characterize long term determinant behaviour of actinide

transport in geological media, requisite to establishing reliable prognoses of proposed nuclear waste disposal sites. Because these studies involve natural systems with inherent heterogeneity (multi-component systems), spatially resolved speciation techniques are essential. Investigations of actinide geological transport in the context of nuclear waste disposal are especially challenging, as an accurate prognosis demands process understanding over an immense time domain. One strategy for meeting this challenge is through investigation of geological natural analogues, which mimic repository geochemical and geological conditions on a geological time scale. Knowledge gained from natural analogues can be used to span the long time scales in a top down approach for predicting repository radiological safety. In order to reliably predict evolution on very long time scales inevitably knowledge of the primary reactions and processes determinant in the fate of radionuclides released into the environment (e.g., sorption, precipitation, solid solution formation reactions) is required, often under non-equilibrium conditions. To this end, as well as for site specific characterisation method development, we investigate actinide transport in column tracer studies, which are models simulating actinide release (plume). The following discussion is divided according to these two major investigative themes. Recent results obtained on a naturally U-rich argillaceous sediment high in organic matter are first presented in detail. Short summaries of results from another natural analogue, which has been studied intensely, and a granite column slice following a radionuclide trace investigation are then presented. These examples should lend an impression of the information available from such spatially resolved investigations. The ultimate goal of these studies is to advance development of thermodynamic/kinetic descriptions used for modelling/prediction of actinide transport processes at varying spatial and temporal scales, with a reliable estimate of uncertainty.

### ***NATURAL ANALOGUE FROM THE PERMIAN LODÈVE BASIN IN FRANCE***

We report our most recent results of spatially resolved X-ray fluorescence and X-ray absorption fine structure investigations with a micrometre-scale resolution ( $\mu$ -XRF and  $\mu$ -XAFS, comprised of the near ionisation threshold energy region, XANES, and the extended energy region, EXAFS) on two uranium-rich clay samples originating from Autunian shales in the Permian Lodève Basin (France), provided by CREGU (Centre de Recherche sur la Géologie des Matières Premières Minerals et Energétiques). This argillaceous formation is a natural U deposit (or mineralisation) associated with organic matter (bitumen) [1, 2]. The goal of this study is to determine the U oxidation state in the sample and to ascertain if any correlation between the U distribution and that of other elements present in the organic-rich fine-grained pelites exists, which might give us insight into the mechanism of U immobilisation through either adsorption/co-precipitation with iron hydroxides and/or clay minerals.

Autoradiographic images and photographs of the samples are shown in Fig. 1. Uranium-rich areas of the sample or hot spots are visible as dark spots in the autoradiographic images.

Quantification of the hot spots shows they contain  $\sim 2$  mg  $^{238}\text{U}/\text{g}$  material (sample marked P31) and  $\sim 25$  mg  $^{238}\text{U}/\text{g}$  material (sample P15).

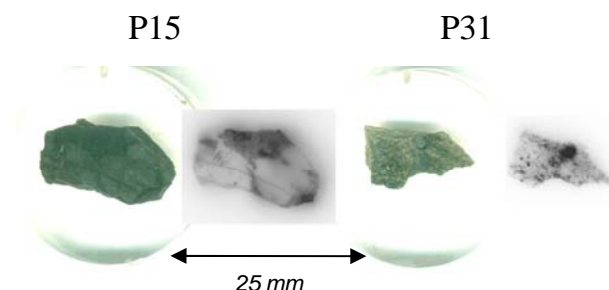


Fig. 1. Photographs of the samples studied embedded in acrylic (designated P15 and P31) and their corresponding radiographic images.

$\mu$ -XRF and  $\mu$ -XANES measurements are recorded at Beamline L at the Hamburger Synchrotron Labor (HASYLAB). A confocal irradiation-detection geometry is used, providing added depth information and allowing probing sample volumes below the surface, thereby avoiding any surface oxidation artefacts caused by cutting and polishing the clay sample. Elemental distribution maps are obtained by means of scanning  $\mu$ -XRF and plotting recorded relative fluorescence intensities for each pixel and scaling them with a linear colour code, with dark pixels corresponding to high count rates. By scanning arbitrary sample areas (x,y scans) at different depths (z) using the confocal setup, stacks of tomographic cross-sections can be easily recorded [3, 4]. Polycapillary half lenses are used for both focussing and collimating optics. The focal spot diameter is approximately 16  $\mu\text{m}$ .  $\mu$ -XRF measurements are recorded using a band pass of wavelengths with an average weighted energy of 17.6 keV delivered by a Mo/Si multilayer pair (AXO Dresden GmbH, Germany) and a Si drift detector (Vortex, SII NanoTechnology USA Inc., Northridge, CA). U L3  $\mu$ -XANES are recorded using monochromatic X-rays at selected sample volumes of high U concentration identified in the  $\mu$ -XRF maps at Beamline L. Both XANES and EXAFS are measured at positions of high U concentration identified by line scans of windowed U  $L\alpha$  counts registered with a high purity Ge detector (Canberra) at the INE-Beamline at the Ångströmquelle Karlsruhe, ANKA [5]. The measured beam spot at the INE-Beamline is 300  $\mu\text{m}$ . Si(111) and Ge(422) crystals are used in the double crystal monochromator at HASYLAB and ANKA, respectively, and the energy is calibrated relative to the first inflection point in the K XANES of a Y foil (defined as 17.038 keV).

The measured distributions for K, Ca, Ti, Fe, Zr, and U in the area with the highest radioactivity at the top of sample designated P15 are shown in Fig. 2. These distributions demonstrate three general observations from this sample: 1) distinct patterns of element distributions are observed, despite the sample's general heterogeneous optical appearance; 2) the U distribution is often correlated with the distributions of lighter weight elements K, Ca,

and Ti (especially notable in the round features in the upper right corner of the maps); and 3) the U distribution is generally inversely correlated to areas of high Fe content.

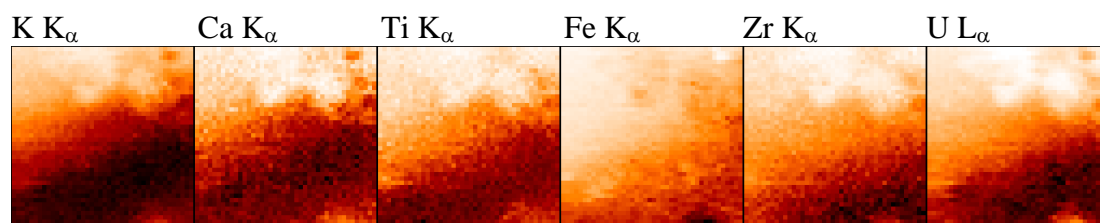


Fig. 2. Distribution maps for the elements indicated in a  $800 \times 760 \mu\text{m}^2$  section ( $20 \times 20 \mu\text{m}^2$  step size), recorded near the surface of sample P15.

A comparison of elemental distributions for an area of sample P31 is depicted in Fig. 3. A red-green-blue (RGB) overlay image of regions exhibiting the highest Ti, Fe, and U fluorescence intensities, respectively, is also shown. We observe a direct correlation between Ti and U, visible as purple areas in the RGB image, but none between Fe and U; the Fe-rich areas remain green in the RGB overlay. As opposed to the positive correlation between Ca and U qualitatively observed in the distributions shown in Fig. 2 for sample P15, no correlation between Ca and U is observed here.

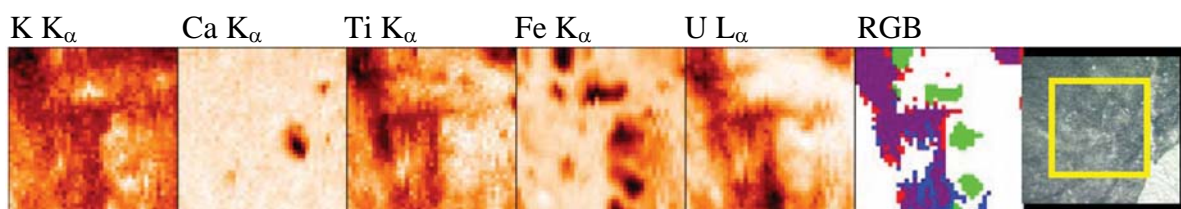


Fig. 3. Distribution maps for K, Ca, Ti, Fe, and U in a  $400 \times 400 \mu\text{m}^2$  section ( $10 \times 10 \mu\text{m}^2$  step size, 1s counting time), recorded under the surface of the P31 sample area marked in the microscope image at far right. A red-green-blue (RGB) overlay image for regions of highest Ti, Fe, and U concentrations is also shown.

In order to determine the valence state of the U in the pelites, U L3  $\mu$ -XANES (Fig. 4) and  $\mu$ -EXAFS (Fig. 5) are recorded at volumes and areas with high U L $\alpha$  intensity. The energy position of the most prominent absorption peak in the XANES (the white line, WL) measured for three different sample regions at two different beamlines all lie within less than 1 eV of that for the U(IV) reference. The XANES features themselves also provide further evidence that the U hot spots contain U(IV). No multiple scattering feature at around 10 eV above the WL,

indicative of U(VI) [6], is observed. We conclude from XANES results in Fig. 4 that U is likely present in the sample in the tetravalent state.

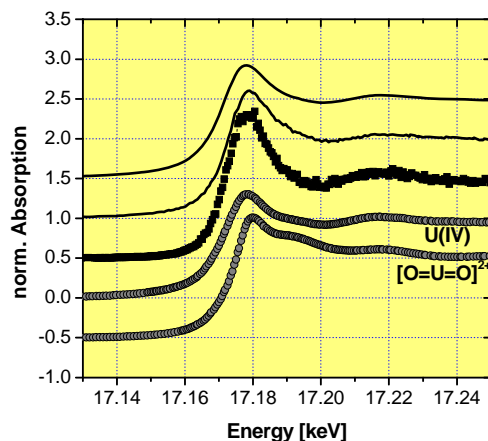


Fig. 4. U L3  $\mu$ -XANES recorded at U hot spots with a microfocus at Beamline L (symbols) and with a 300  $\mu\text{m}$  beam spot at the INE-Beamline at ANKA (lines) compared to two U(IV) and U(VI) reference spectra (bottom).

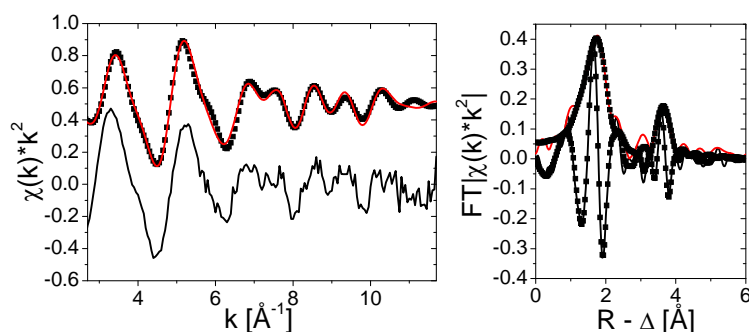


Fig. 5. U L3  $k^2$ -weighted EXAFS ( $\chi(k)$ ; left bottom), Fourier-filtered data and best fit result (left top) and corresponding  $k^2$ -weighted Fourier transform (FT) data (right) plotted with best fit results. Experimental data = lines. Fit curves = symbols.

This interpretation is corroborated by the U L3 EXAFS spectrum (Fig. 5). The data is well fit beginning with a structural model similar to uraninite,  $\text{UO}_2$  [7]. Best results are obtained with 4-5 O atoms at 2.29  $\text{\AA}$  with  $\sigma^2 = 0.013 \text{ \AA}^2$  and 2-3 U atoms at 3.78  $\text{\AA}$  with  $\sigma^2 = 0.008 \text{ \AA}^2$ . The distances are 2 - 3 % smaller than expected for  $\text{UO}_2$  and the intensities lead to a much smaller coordination number than expected ( $N(\text{O}) = 8$ ;  $N(\text{U}) = 12$ ). This may indicate the  $\text{UO}_2$ -like phase is present as a nano-particulate material with large surface area having relaxed (shortened) distances at the surface. Note that no short U-O distance expected for the U(VI) uranyl moiety is found in the EXAFS spectrum [6].

We conclude from this investigation that the U in this clay formation is tetravalent. In the area investigated with EXAFS it found to be present as a UO<sub>2</sub>-like phase but likely nanocrystalline. Future planned spatially resolved X-ray diffraction investigations of the same samples may help confirm this. The distribution of U is observed to be inversely correlated to the Fe distribution and associated with lighter weight elements. Scanning transmission X-ray spectro-microscopy (STXM) studies using carbon K-edge, K L-edge and Fe L-edge XANES reveal a positive K correlation with organic carbon and a negative correlation of organic carbon with Fe. This may indicate that the organic material associated with illite-type clay minerals identified by XRD acted as reducing agent during U immobilisation. More study is needed to develop a more complete model for a U immobilisation scenario.

### ***NATURAL ANALOGUE RUPRECHTOV***

We have also investigated U-rich argillaceous Tertiary sediment bore core sections originating from the natural analogue Ruprechtov site in the Czech Republic using micro-focussed synchrotron radiation in recent years. Similar to the U-rich clay study described above, the aim is to assess mechanisms leading to U immobilisation by determining the U speciation in the sediment and characterising its spatial distribution relative to other elements and mineral phases. Chemical state maps of As are recorded in our investigations by scanning with excitation energies, which selectively ionize single oxidation states, in this case selectively exciting As(0) or As(V). Both XANES and EXAFS spectroscopy is used for characterising chemical speciation and scanning diffraction techniques for mineral phase distribution mapping.

Measurements are recorded at Beamline L at HASYLAB, at the Fluo-Topo Beamline at ANKA, and at ID22 at the European Synchrotron Radiation Facility, ESRF. Various X-ray imaging (reflective and refractive) micro-focussing optics are used: polycapillary lenses, new planar compound refractive lenses (CRL) fabricated at FZK's Institute for Microstructure Technology (IMT) [8], and Kirkpatrick-Baez (KB) mirrors. Most measurements are performed in a confocal irradiation-detection geometry, providing added depth information.

We summarize the results from these investigations [3, 9-11] in the following. Uranium U L3  $\mu$ -XANES results (Fig. 6) reveal uranium in the sediment to be present in tetravalent form. Analysis of a  $\mu$ -EXAFS spectrum (Fig. 7) recorded below the sample surface to avoid oxidation artefacts on the surface from cutting the bore column shows the U(IV) phase to be a U-phosphate/sulphate. The presence of uraninite observed in bulk XRD and EDAX is confirmed from  $\mu$ -XRD measurements on thin section samples.

The analyses of a number of tomographic cross-sections of elemental distributions recorded over different sample areas with around 15 to 20  $\mu$ m resolution shows a strong correlation between U and As. Arsenic K-edge  $\mu$ -XANES measurements reveal As to be present mostly as As(0), with some As(V); no As(III) is found. From comparison of measured

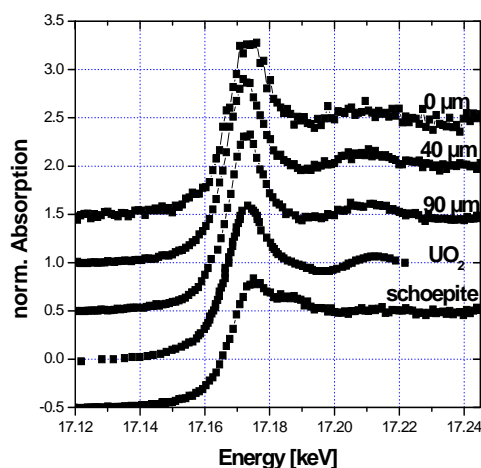


Fig. 6. U L3  $\mu$ -XANES recorded at various positions of the bore core section, at different depths below the surface indicated, and compared to U(IV) and U(VI) reference sample XANES.

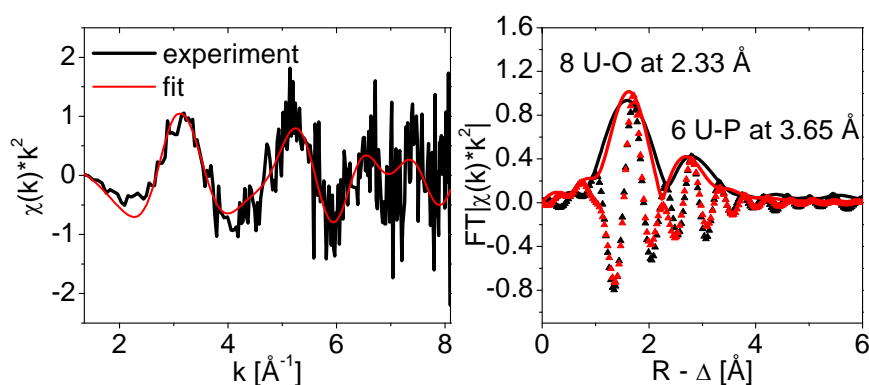


Fig. 7. U L3  $\mu$ -EXAFS (left) and corresponding Fourier transformed data (right; magnitude in solid lines and imaginary part as symbols). Experimental data is shown in black and the fit result in red.

U, As(0), and As(V) distributions, a positive correlation between U and As(V) is found. The As K-XANES of As(0)-rich areas in the sample show a fingerprint comparable to that for arsenopyrite, AsFeS. A linear correlation between As(0) and Fe observed in elemental distribution maps supports the presence of AsFeS. Further evidence of AsFeS is seen in distribution maps recorded with a high lateral resolution (2  $\mu$ m), where an As-rich boundary layer or rim surrounding Fe framboidal nodules is observed (Fig. 8). Uranium occurs in direct vicinity of these As-rich boundary layers.

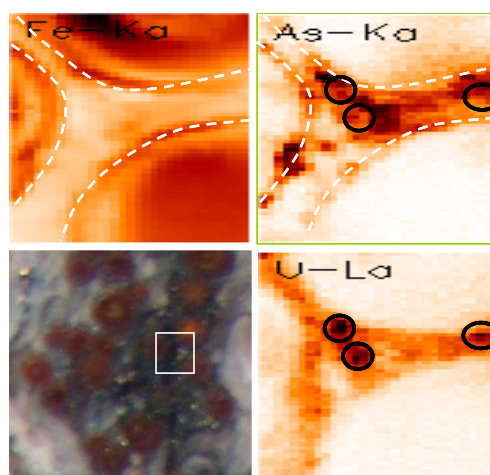
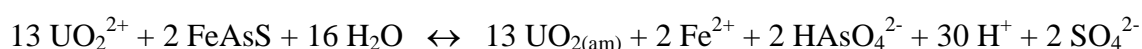


Fig. 8. Confocal  $\mu$ -XRF maps of a  $120\ \mu\text{m} \times 120\ \mu\text{m}$  section ( $2\ \mu\text{m} \times 4\ \mu\text{m}$  v  $\times$  h step size; 15 s counting time),  $-60\ \mu\text{m}$  below the surface, recorded at ANKA. Circles indicate U hot-spots found in the U map. Dashed lines indicate an As-rich rim around a Fe(II)-nodule. The marked region in the microscopic image shows the area studied.

Upon comparison of As distribution maps with scanning  $\mu$ -XRD results (Fig. 9) we find As to be associated with pyrite. We find no XRD evidence for  $\text{AsFeS}$ , indicating that arsenopyrite is present as thin amorphous or nanocrystalline coating on pyrite framboids, which formed secondary to the original framboid nodules. The observation that both pyrite and siderite occur in the same sediment allows us to assume that the pH was near neutral during formation of these minerals.

These results together allow us to formulate one of the mechanisms for U-enrichment in the sediment. The  $\text{AsFeS}$  in the sediment reduced mobile groundwater-dissolved U(VI) to less-soluble U(IV), thereby immobilising the uranium as U(IV). As a consequence As(V) was formed. In formulating a general reaction scheme we use doubly deprotonated arsenic acid ( $\text{pK}_{\text{a}2} = 6.8$ ) for near neutral pH conditions:



The Gibbs free energy,  $\Delta_r G^0$ , for this reaction is estimated to be around  $-43\ \text{kJ/mol}$ , which is an exothermic reaction.

### **TRACER STUDY OF ÄSPÖ GRANITE**

We investigate Np speciation and spatial distribution in a fractured granite bore section from the Swedish Äspö Hard Rock Laboratory following a radiotracer experiment [12]. A polished slice of a fractured granite bore core column (52 mm in diameter) used in a radiotracer experiment is studied. The actinide tracer cocktail contained long-lived radioisotopes,

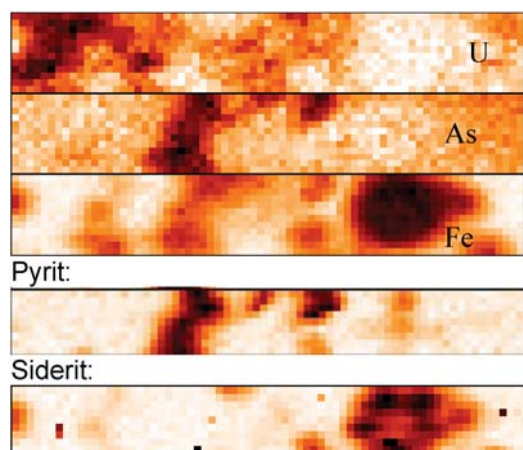


Fig. 9. Top: Fe, As, and U distributions in a  $710 \mu\text{m} \times 120 \mu\text{m}$  thin section ( $10 \mu\text{m} \times 10 \mu\text{m}$ , counting time = 10 s).  
Bottom: Distribution of measured diffraction intensities for d-spacings expected reflexes for pyrite and siderite for the first 9 rows (i.e. top  $90 \mu\text{m}$ ) of the distribution images. The darker the pixel the higher the measured intensity in all images.

including  $10^{-5} \text{ mol/dm}^3$   $^{237}\text{Np}$  (added as  $\text{Np(V)}$ ). The slice studied is where most of the tracer activity was recovered and contains  $\sim 3 \text{ nmol Np/g}$ ;  $< 1 \text{ ppm}$ ).

Analysis of  $\text{Np L3 } \mu\text{-XANES}$  results (Fig. 10) allows us to conclude that  $\text{Np}$ , originally introduced as  $\text{Np(V)}$  onto the column, is reduced to  $\text{Np(IV)}$  in the fractured granite. We note that without the spatial resolution of the experimental setup and the confocal geometry it would not have been possible to obtain this information on such a dilute tracer concentration. Use of confocal geometry is especially important in these experiments as probing volumes below the sample surface not only avoids potential speciation changes caused by sample preparation, it also limits the sample volume probed, which minimizes spectral interference from other elements (in this case energetically close lying  $\text{Np L}_{\alpha 1}$  and  $\text{Sr K}_{\alpha 1}$  emission lines).

The distribution of  $\text{Np(IV)}$  is apparently associated with  $\text{Zn}$  (Fig. 11). We assume that this indicates that  $\text{ZnS}$  played a role in  $\text{Np(V)}$  reduction to  $\text{Np(IV)}$  and subsequent immobilisation as the less soluble tetravalent form. There are sample areas where a correlation between  $\text{Np}$  and  $\text{Fe}$  is observed, but there are other areas with none (Fig. 11). The correlation between  $\text{Np}$  and  $\text{Fe}$  may indicate one or both of two things:  $\text{Np(V)}$  was immobilized by reduction by  $\text{Fe(II)}$  and/or the  $\text{Np}$  is located in fissures, as  $\text{Fe}$  is an indicator element for granite fracture material. The sample regions, where no correlation between  $\text{Fe}$  and  $\text{Np}$  is found, may be associated with fissures, which either are not easily accessible by inflowing groundwater carrying the  $\text{Np}$  tracer or have flow rates too high for slower kinetic reactions to occur.

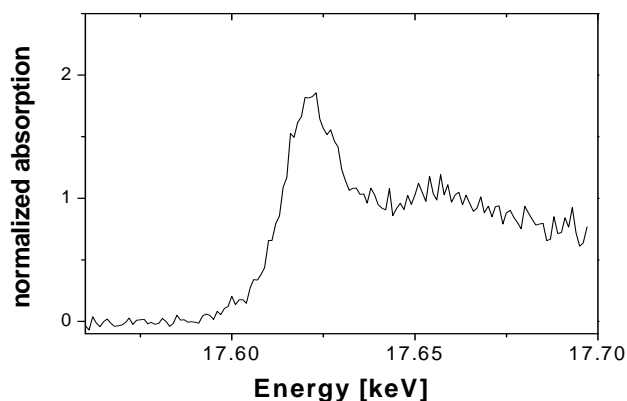


Fig. 10. Np L3  $\mu$ -XANES measured at a Np hot spot around  $-50 \mu\text{m}$  below the sample surface. Inset: Np(IV) and Np(V) reference spectra.

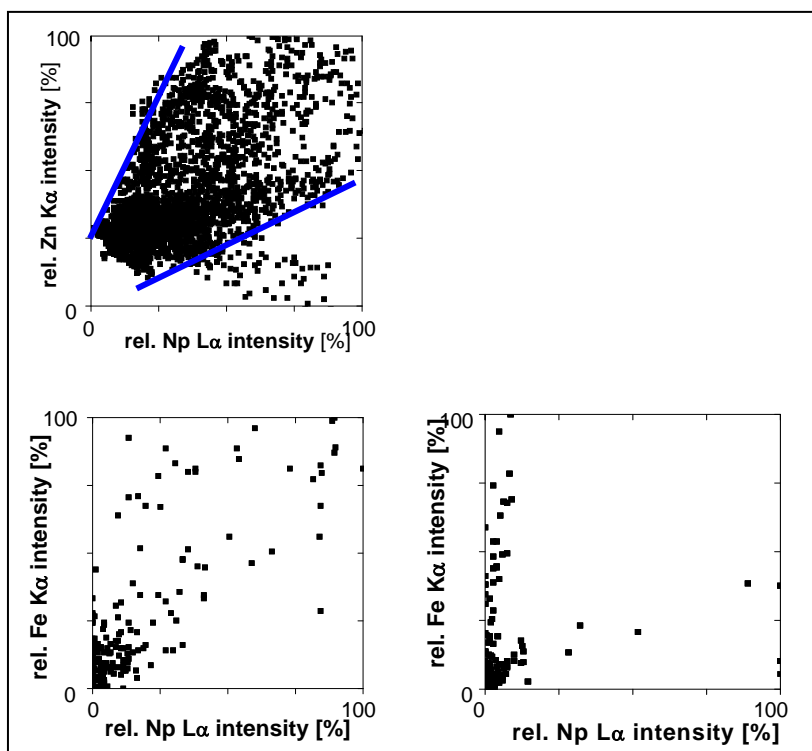


Fig. 11. Correlation plots created using normalized fluorescence intensities between Zn and Np (left) and between Fe and Np using two different maps (bottom). Lines with slopes  $\frac{1}{2}$  and 2 in top figure are a guide to the eye.

The distribution of Np(IV) is apparently associated with Zn (Fig. 11). We assume that this indicates that ZnS played a role in Np(V) reduction to Np(IV) and subsequent immobilisation as the less soluble tetravalent form. There are sample areas where a correlation

between Np and Fe is observed, but there are other areas with none (Fig. 11). The correlation between Np and Fe may indicate one or both of two things: Np(V) was immobilized by reduction by Fe(II) and/or the Np is located in fissures, as Fe is an indicator element for granite fracture material. The sample regions, where no correlation between Fe and Np is found, may be associated with fissures, which either are not easily accessible by inflowing groundwater carrying the Np tracer or have flow rates too high for slower kinetic reactions to occur.

The highest Np concentrations were found clustered in 1 - 3 pixels (pixel size of 20  $\mu\text{m}$  or 10  $\mu\text{m}$ ) of scanned areas associated with small granite fissures of less than 100  $\mu\text{m}$  width (Fig. 12). That high activity is localized in the smallest fissures may indicate that during the tracer experiment inflowing Np has a shorter residence time in large fractures, while in the small fissures migration is slower, leading to longer residence times, i.e., reaction times, resulting in Np(V) reduction and immobilisation to less soluble Np(IV). That a clustering of pixels with high Np intensity can be interpreted as either formation of precipitate or presence of a sorbed species at highly localized areas on the fissure walls.

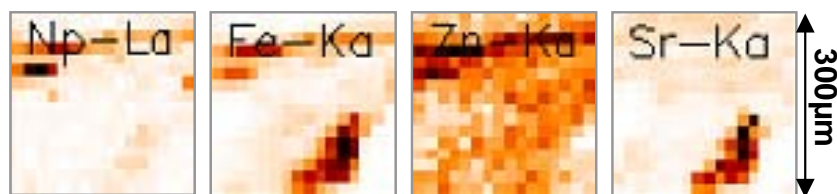


Fig. 12.  $\mu$ -XRF distribution maps recorded in confocal geometry for Np, Fe, Zn, and Sr of a 300 x 300  $\mu\text{m}^2$  section ( $20 \times 20 \mu\text{m}^2$  step size; 7 s counting time) of the granite core slice  $\sim 40 \mu\text{m}$  below the surface.

This study has implications for modelling scenarios of actinide release in a nuclear waste repository placed in a granite host rock formation. The redox conditions of the groundwater/granite obviously play a role, but this is coupled to varying hydrological transport affected by the size and interconnectivity of the fractures and fissures in the granite.

### OUTLOOK

We are presently installing the necessary equipment and instrumentation for achieving a beam focus in the micrometre range at the INE-Beamline for actinide research at ANKA. Two different focussing optics have been already tested, CRLs fabricated by FZK-IMT and a polycapillary focussing half lens (on loan from HASYLAB). First experimental results of the setup are expected in 2008.

Entirely new possibilities will open up for spatially resolved investigations when the hard X-ray micro/nano probe beamline at the highly brilliant and coherent PETRA III at HASYLAB

becomes operational (beamline installation begins in 2009). This beamline will provide focussed X-ray beams with micrometre and sub-micrometre or nanometre beam spot dimensions for high spatial resolution with increased sensitivity [13]. The brilliance is especially beneficial to tracer studies, in order to optimize lower detection limits.

### ACKNOWLEDGEMENTS

We acknowledge ANKA, the ESRF, and HASYLAB for allocation of beamtime and the institutions somehow involved in development of a micro-focus INE-Beamline (IMT, ISS, ITU, and HASYLAB). We also thank Ms. Eva Soballa for mounting and preparing samples and Dr. J. Römer for the autoradiographic measurements.

### REFERENCES

- [ 1] C. Marignac and M. Cuney (1999) *Mineralium Deposita*, **34**, 472.
- [ 2] V. Mathis, J.-P. Robert and J. Saint Martin (1990) *Chron. Rech. Min.*, **499**, 31.
- [ 3] M.A. Denecke, K. Janssens, K. Proost, J. Rothe and U. Noseck (2005) *Environ. Sci. Technol.*, **39**, 2049.
- [ 4] K. Janssens, K. Proost and G. Falkenberg (2004) *Spectrochim. Acta B*, **59**, 1637.
- [ 5] M.A. Denecke, J. Rothe, K. Dardenne, H. Blank and J. Hormes (2005) *Physica Scripta*, **T115**, 1001.
- [ 6] M.A. Denecke (2006) *Coord. Chem. Rev.*, **250**, 730.
- [ 7] R.H. Rundel, N.C. Baenzinger, A.S. Wilson and R.A. McDonald (1948) *J. Amer. Chem. Soc.*, **70**, 99.
- [ 8] V. Nazmov, E. Reznikova, M. Boerner, J. Mohr, V. Saile, A. Snigirev, I. Snigireva, M. DiMichiel, M. Drakopoulos, R. Simon, and M. Grigoriev (2004) *AIP conference proceedings*, **705**, 752.
- [ 9] M.A. Denecke, K. Janssens, B. Brendebach, W. De Nolf, G. Falkenberg, J. Rothe, R. Simon, A. Somogyi, B. Vekemans and U. Noseck (2007) *X-ray absorption fine structure*. in: XAFS13 (B. Hedman and P. Pianetta, Eds.). American Institute of Physics, Melville, NY, 187-189.
- [10] M.A. Denecke, A. Somogyi, K. Janssens, R. Simon, K. Dardenne and U. Noseck (2007) *Microscopy Microanal.*, **13**, 165.
- [11] M.A. Denecke, W. De Nolf, K. Janssens, B. Brendebach, A. Rothkirch, G. Falkenberg and U. Noseck (2008) *Spectrochim. Acta B*, in print.
- [12] J. Römer, B. Kienzler, P. Vejmelka, E. Soballa, A. Görtzen and M. Fuss (October 2002) *FZK-Wissenschaftliche Berichte*, FZKA6770.
- [13] G. Falkenberg, N. Reimers and Chr. Schroer (2007) *Status of the hard X-ray micro/nano-probe beamline (P06) at Petra III. HASYLAB Annual Report 2007*, 185.